Colloid and Polymer Science (2024) 302:609–622
https://doi.org/10.1007/s00396-023-05218-7

RESEARCH

Mechanical behavior of polyamide-6 after combined photo-oxidative and hygrothermal aging

K. N. Cundiff[1,2] · A. K. Rodriguez[3,4] · A. A. Benzerga[1,3]

Received: 2 October 2023 / Revised: 5 December 2023 / Accepted: 12 December 2023 / Published online: 27 December 2023

Abstract

The effect of moisture on the photo-oxidative degradation of polyamide-6 (PA-6) was studied by analyzing the mechanical response after two different accelerated aging procedures. In the first aging procedure, the PA-6 was only exposed to ultra-violet (UV) radiation at 60 °C. In the second procedure, the same duration of UV radiation was periodically interrupted while the relative humidity was raised to 100%. Diffusion-limited and nominally homogeneous degradation conditions were investigated using bulk and film specimens, respectively. Accelerated UV aging reduced the ductility of PA-6, but the additional hygrothermal exposure had no effect on the ductility or strength, indicating that humidity did not influence the photo-oxidation of PA-6. This finding contrasts with previous studies that found thermo-oxidation of PA-6 was accelerated by moisture.

Keywords Semicrystalline thermoplastics · Polyamide · Photo-oxidation · Hygrothermal aging · Coupled aging

Introduction

Harsh environmental conditions can initiate chemical reactions in polymers that degrade their mechanical properties over time, in a process sometimes called chemical aging. Chemical aging limits the lifetime of polymer parts, with the most critical effect typically being a catastrophic loss of ductility, i.e., embrittlement. Therefore, lifetime predictions for polymers deployed under harsh environments depend on a thorough understanding of chemical aging.

✉ K. N. Cundiff
kcundif@sandia.gov

A. K. Rodriguez
akr.atencio@gmail.com

A. A. Benzerga
benzerga@tamu.edu

[1] Department of Aerospace Engineering, Texas A&M University, College Station 77843, TX, USA

[2] Sandia National Laboratories, Albuquerque 87185, NM, USA

[3] Department of Materials Science and Engineering, Texas A&M University, College Station 77843, TX, USA

[4] Department of Mechanical Engineering, Texas A&M University at Qatar, Doha, Qatar

The adjective "harsh" may evoke thoughts of extraordinary environments such as outer space [1], directed UV to sterilize a surface [2], or the high temperatures in the engine of a car [3], but normal, outdoor environments are also sufficiently "harsh" to provoke chemical aging [4–9]. One obstacle to predicting lifetime limits imposed by chemical aging is that, within a single environment, there may be a number of different conditions that each cause their own pathway for chemo-mechanical degradation. For instance, most natural environments simultaneously experience some combination of UV radiation, high temperatures, and humidity, and these factors typically cause photo-oxidation [5, 10], thermo-oxidation [11, 12], and hydrolysis [13], respectively.

Chemical aging is commonly studied under laboratory conditions where a single degradation pathway is isolated, and changes in either macromolecular indicators (e.g., molecular weight, interlamellar spacing) or mechanical properties (e.g., strain-to-failure, ultimate tensile strength) are measured as a function of exposure to the controlled environment [14–22]. While this approach has laid a solid foundation for understanding specific degradation pathways, there is uncertainty associated with deploying these findings to predict polymer lifetimes in real environments. First, it is not straightforward to map accelerated aging conditions onto natural

aging conditions [18], and, second, natural environments almost always contain multiple factors that might induce coupled aging mechanisms [23–25].

On the other hand, many studies adopt an engineering approach where polymers are aged under their real service environment [4, 6–8, 26, 27].[1] The engineering approach provides actionable information for a single polymer system aged in a single environment, but results are not easily transferable to other materials or environments. Furthermore, real-time aging experiments are expensive due to the long times required. Although using a real service environment to age a polymer guarantees exposure to the relevant environmental factors, the lack of control over each factor makes it difficult to precisely determine coupling between them.

So far, only a few studies have characterized chemical aging using controlled environments that combine multiple instigators for chemical aging in order to investigate the potential nonlinear coupling between various degradation pathways. However, the subset of studies that do explore multiple aging mechanisms tend to focus on polyamide-6 (PA-6) or polyamide-6,6 (PA-6,6), since the kinetics of individual degradation pathways in these polymers are well understood [12, 13]. In PA-6, water can initiate a hydrolysis reaction that attacks the amide group. This causes chain scission between the C–N bond, leaving behind two chain ends with carboxylic acid and amine end groups [13]. The reactions for photo-oxidation and thermo-oxidation are very similar, and their processes are common for many thermoplastic polymers [10]. Their two main differences are the energy source that dissociates bonds in the initiation step of the auto-oxidation cycle [10] and the longevity of intermediate products due to their respective photo- and thermal-stability [28]. Oxidation can result in both chain scission and cross-linking, although chain scission is predominant in thermoplastics when oxygen is present [10]. Chain scission is often realized by breaking C–C bonds in the polymer backbone. This is usually achieved by the scission of alkoxy radicals ($PO^{\cdot}$) or the decomposition of hydroperoxides (POOH). Both of these processes leave behind carbonyl end groups (C=O) [10]. In PA-6, chain scission by oxidation can create imides that are susceptible to hydrolysis [29]. The creation of hydrolyzable imides on the polymer backbone is one proposed mechanism for the acceleration of oxidation in the presence of water, but the exact mechanism for coupling, or even whether water accelerates degradation, is not entirely clear.

Bernstein et al. [23, 30] measured the decreasing tensile strength of PA-6,6 after exposure to either dry air or air at 100% relative humidity (RH). They found that the main degradation pathway of PA-6,6 under 100% RH and oxygen was essentially hydrolytic, consistent with the fact that their PA-6,6 fibers contained anti-oxidant additives, and also that oxygen accelerated hydrolytic degradation for temperatures above 50 °C. In contrast, Gonçalves et al. [31] found that, between 25 and 90 °C and for aging times of two days, the main degradation pathway of additive-free PA-6,6 in water with oxygen was thermo-oxidation. They characterized the state of degradation by measuring changes in the IR bands using FTIR and solid-state ^{13}C NMR spectroscopies. They concluded that water accelerated thermo-oxidation, not by acting as a reactive species, but through sorption of water that increased the PA-6,6 chain mobility. Molecular dynamics simulations have also shown that increasing moisture content accelerates the thermal degradation of PA-6,6 [32].

More recently, Deshoulles et al. [25] studied chemical coupling between oxidation and hydrolysis in PA-6 films. They observed that at 80 °C the chain scission rate of PA-6 in water with oxygen was 80× faster compared to PA-6 in water without oxygen. Furthermore, when the PA-6 films were thermo-oxidized at 100 °C in dry air at prior to being hydrolyzed at 100 °C in water without oxygen, longer pre-oxidation treatments corresponded with a higher chain scission concentration during the hydrolysis step. They concluded that nonlinear coupling between thermo-oxidation and hydrolysis between 80 and 100 °C arises from the formation of imides during oxidation [25]. Since the imides are susceptible to hydrolysis, oxidation essentially creates more sites on the polymer chain that are susceptible to hydrolysis. However, not all polymers are expected to exhibit nonlinear coupling between thermo-oxidation and hydrolysis. For example, Bahrololoumi et al. [33] proposed a constitutive model for hygrothermally aged cross-linked polymers where thermo-oxidative and hydrolytic degradation were assumed superposable (i.e., not coupled). The model successfully predicted the constitutive behavior of hygrothermally aged neoprene and ethylene propylene diene monomer (EPDM) rubber after several different hygrothermal aging histories.

Of the studies on coupled degradation mechanisms, those on combined UV and hygrothermal aging are scarce. Roger et al. [29] found that photo-oxidation at long-wavelengths (> 340nm) also lead to the formation of imides and that water consumed these imides through hydrolysis. They also found that the imides in PA-6 were less stable than in PA-11 or PA-12. In [24], it was found that moisture had no influence on the photo-oxidation of PA-6 films (50 µm thick), as measured by the carbonyl absorbance. Ishida et al. [34] studied the photo-oxidation at 60 °C of an acrylic-urethane network (AUN) polymer under dry (< 10% RH) and wet (75% RH) conditions. They found that water delayed the reactions

[1] Sometimes, the use of a real environment, especially a natural one, to study degradation is called weathering instead of chemical aging. This is because a natural environment will likely degrade a polymer from both chemical and non-chemical effects. Some examples of non-chemical degradation include abrasion from dust particles blown in the wind or the absorption of water by a hygroscopic polymer.

associated with photo-oxidation. The mechanism proposed for this delay was a reduced concentration of hydroperoxide (POOH) in the presence of water, which is a key intermediate for the photo-oxidation of AUN. Furthermore, under dry conditions, photo-oxidation resulted in homogeneous degradation of the AUN polymer by crosslinking, but wet photo-oxidation resulted in heterogeneous degradation where chain scission was predominant overall, but some sub-nanoscale domains were crosslinked [34].

The goal of the present study is to characterize the mechanical behavior of a semicrystalline thermoplastic after coupled UV and hygrothermal chemical aging. The body of work on coupled aging mechanisms in thermoplastics is relatively small and focuses on hygrothermal aging (hydrolysis and/or thermo-oxidation) [23–25, 30–32]. There are very few studies on coupled photo-oxidation and hygrothermal aging [24, 29], none of which discuss mechanical behavior. Furthermore, the studies on coupled photo-oxidative and hygrothermal aging [24] report conclusions at odds with the studies on coupled thermo-oxidative and hygrothermal aging [23, 25], where moisture is found to accelerate thermo-oxidative degradation, but not photo-oxidative degradation, despite the two reactions only differing by the energy source that initiates the reaction [10, 11]. This investigation uses polyamide-6 (PA-6), which was chosen because its oxidative and hydrolytic degradation have been extensively studied [12, 13, 17, 22].

Experimental methods

Material

Experiments used additive-free PA-6 in bulk and film form. Both bulk and film materials originate from the same batches described in previous studies [20, 35]. Bulk tensile specimens were machined from a 0.5 in (12.7 mm) thick plate of PA-6 from Plastics International. In a previous study [20], the crystal mass fraction and glass transition of the plate were measured as 38±1% and 47±4 °C using differential scanning calorimetry (DSC). The DSC characterization used specimens with masses from 4 to 6 mg tested in a TA Instruments Q20 DSC with a protocol of heating from 25 to 250 °C at a rate of 5 °C/min under nitrogen gas [20]. Right cylindrical bars were machined from the PA-6 plate using a lathe. The bars had a total length of 73.03 mm, a gauge length of 12.70 mm, a gauge diameter of 4.76 mm, and a grip diameter of 7.94 mm. Films with thickness 0.06 mm were obtained from Goodfellow, also with a crystal mass fraction of 38 ± 1%. The DSC characterization of the films was also reported in a previous study [20] and used the same procedure described above for the bulk specimens, except that the measurements were made using a PerkinElmer Pyris 1 DSC. Tensile specimens were cut from the film sheets using a punch. The film specimens had a double fillet, a total length of 75 mm, a gauge length of 6 mm, and a gauge width of 4 mm.

Aging

To compare coupling between photo-oxidation and water, PA-6 specimens were either aged by UV radiation or by alternating UV radiation and 100% relative humidity (RH). The aging procedures were based on ASTM G154-12a [36]. UV-only aging was conducted in a QUV Accelerated Weathering Tester using fluorescent UVA bulbs with a spectral irradiance of 1.55 W/(m^2·nm) at the nominal peak wavelength of 340 nm. The aging occurred at a chamber temperature of 60 °C and ambient humidity. Nominal exposure times from 48 to 192 h were used. To evenly irradiate the surface of the bulk specimens, they were periodically rotated by 120° every 8 h. Each 120° section of the lateral surface was aged for the full nominal aging time. Therefore, bulk specimens UV-aged for nominally 48, 96, and 192 h spent 144, 288, 576 h under irradiation from the UVA lamps. On the other hand, the thickness of the films was less than the nominal depth of diffusion-limited oxidation (DLO) [10, 19, 37, 38], so they were not rotated or flipped during aging. UV-only aging procedures are described using a shorthand, where "UV" is followed by the nominal UV exposure time, e.g., UV48 denotes 48 h of UV exposure.

During the combined UV and hygrothermal aging protocol, the weathering tester alternated between UV exposure for 24 h and hygrothermal exposure for 4 h. The UV aging periods followed the same procedures as previously described for UV-only aging. During the hygrothermal aging periods, the UV lamps were turned off, the temperature was maintained at 60 °C, and the relative humidity was increased to 100%, i.e., the condensing humidity. Since the bulk specimens were rotated to ensure even irradiation of their surface, they were in the weathering device three times longer than the films to achieve the same nominal UV exposure time. Therefore, due to the fixed duration of the UV and hygrothermal cycles, the bulk specimens were hygrothermally aged for three times as long as the films for a given nominal UV exposure time. For the bulk specimens, for every 24 h of UV exposure, there were 12 h of hygrothermal exposure. For the films, for every 24 h of UV exposure, there were 4 h of hygrothermal exposure. The combined hygrothermal and UV aging regimens are described using a shorthand where "HUV" is followed by the nominal UV exposure time, e.g., HUV48 for 48 h of UV exposure with 24 h of hygrothermal exposure for a bulk specimen and 8 h of hygrothermal exposure for a film specimen. This shorthand naming convention helps correlate aging regimens with the same UV aging time, e.g., UV48 and HUV48 conditions have both been exposed

Table 1 Summary of aging conditions for bulk and film specimens, the amount of energy directed at the specimen for a given duration of UVA lamp exposure, and the number of specimens aged under those conditions

Aging regimen	UV energy (MJ/m^2)	Round specimens			Film specimens		
		UV (h)	Hygro. (h)	Specimens	UV (h)	Hygro. (h)	Specimens
UV48	13	48	0	2	48	0	8
HUV48	13	48	24	3	48	8	6
UV96	27	96	0	2	96	0	8
HUV96	27	96	48	3	96	16	8
UV192	54	192	0	2	—	—	—
HUV192	54	192	96	3	—	—	—

to 48 h of aging, but the HUV48 specimen was subjected to additional hygrothermal exposure. Table 1 summarizes the aging conditions used in this study for both bulk and film specimens. For each aging condition, Table 1 lists the nominal UV and hygrothermal exposure times, the energy directed at the specimen during the UV exposure time, and the number of specimens aged. The specimens were exposed to amounts of UV energy that correspond to approximately 1 week to 1 month of UV energy from natural sunlight in the Middle East [39, 40].

Moisture control

PA-6 is hygroscopic, and its mechanical behavior is sensitive to absorbed moisture [41–43]. To control the moisture content in the specimens, they were dried in a vacuum oven immediately prior to testing. The specimens were dried for 72 h at 80 °C in a Napco model 5831 vacuum oven with the vacuum being maintained by a Welch-Ilmvac Duoseal 1400B-01 pump. A vacuum environment was used to avoid thermo-oxidation [12]. The importance of drying the specimens prior to testing is illustrated in the Appendix.

Mechanical testing

The specimens were tested on an MTS Insight Electromechanical Testing System that was operated in displacement control mode. A 30-kN load cell was used to measure the force on the bulk specimens, and a 1-kN load cell was used to measure the force on the films. Unless otherwise indicated, specimens were loaded at a nominal strain rate of $\dot{\delta}/L_0 = 10^{-3}/\text{s}$, where δ is the crosshead displacement and L_0 is the initial gauge length of the specimen. Tests were conducted at room temperature (24 °C).

Specimen deformation was measured using contour tracking [20], a non-contact, video-based extensometry method. Contour tracking analyzes images from a video of the mechanical test to determine the lateral contractions of the specimen at its narrowest point and then uses this measurement to calculate the true strain in the specimen assuming incompressible deformation, no lateral strain gradients, and transverse isotropy. In the round specimens, the true (Hencky) strain is approximated as

$$\varepsilon = 2\ln\left(\frac{\Phi_0}{\Phi}\right), \tag{1}$$

where Φ_0 and Φ are the initial and current diameters of the specimen. In the right cylindrical bars, the true axial stress is calculated as

$$\sigma = \frac{F}{A} = \frac{4F}{\pi\Phi^2}, \tag{2}$$

where F is the force measured by the load cell and A is the current cross-sectional area. In the films, the true (Hencky) strain and axial stress are approximated as

$$\varepsilon = 2\ln\left(\frac{W_0}{W}\right), \quad \sigma = \frac{F}{A} = \frac{F}{A_0\left(W/W_0\right)^2}, \tag{3}$$

where W_0 and W are the initial and current widths of the film.

Results

Film specimens

The combined effects of photo-oxidation and hygrothermal aging on PA-6 were studied by comparing the mechanical behavior of UV-aged specimens to the mechanical behavior of specimens aged under alternating UV radiation and hygrothermal conditions (abbreviated henceforth as HUV aging). By comparing the mechanical behavior of UV-aged and HUV-aged specimens with the same UV aging time, differences in mechanical behavior can be attributed to the hygrothermal part of the HUV aging procedure.

First, consider PA-6 film specimens, where the thickness is small enough to assume that reactive species are homogeneously distributed throughout the volume during aging. Put simply, diffusion-limited oxidation (DLO) [18] and diffusion-limited hydrolysis (DLH) [44] are not relevant when aging the films. However, the unattenuated photons

Fig. 1 Representative stress–strain curves for PA-6 films aged by UV (blue, solid line) or by alternating UV and hygrothermal conditions (HUV, orange, dashed line). Markers indicate the strain-to-fracture. All specimens were UV-aged for 48 h. Each plot shows results from tests using the same nominal strain rate. The hygrothermal exposure had no apparent effect on the strength of the films

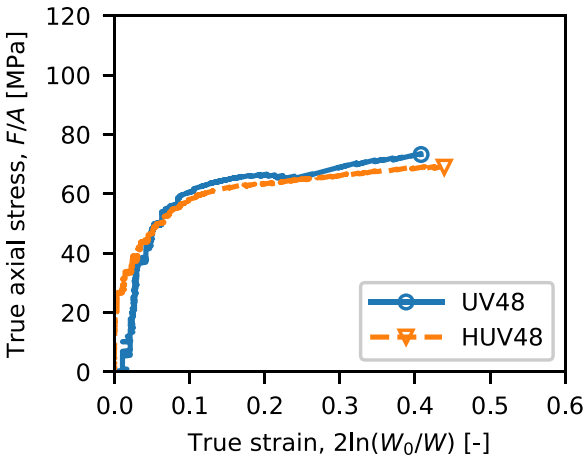

(a) $\dot{\delta}/L_0 = 10^{-3}/\mathrm{s}$

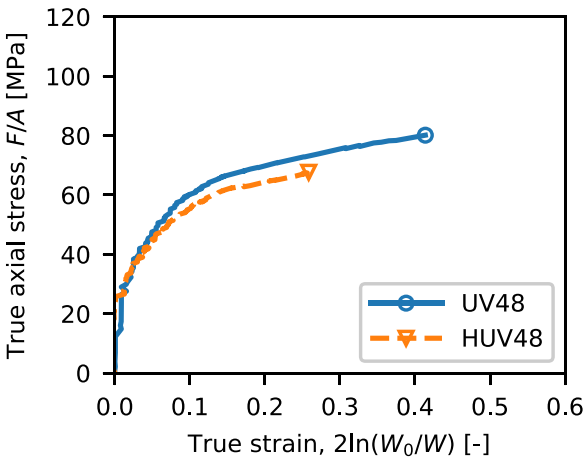

(b) $\dot{\delta}/L_0 = 10^{-2}/\mathrm{s}$

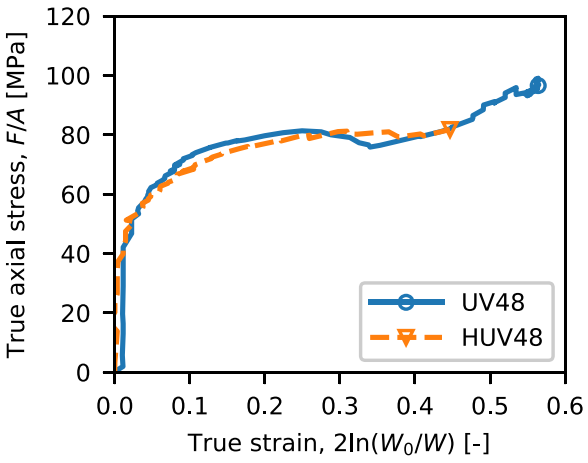

(c) $\dot{\delta}/L_0 = 10^{-1}/\mathrm{s}$

impinging on the surface of the films are expected to create a highly oxidized layer on the order of 1 μm that is not an effect of oxygen diffusion [45].

The same film materials and UV aging procedures were used in a previous study [20]. In that study, it was found that 48 h of UV exposure increased the yield stress of the material, but reduced the strain-to-fracture by roughly a factor of two. After 96 h of UV exposure, the ductility gradually decreased while the yield stress stayed the same. Finally, after 192 h of UV exposure, the material was extremely brittle and fractured well before the onset of any plastic deformation. In the present study, the materials were also exposed to UV and hygrothermal aging to explore whether water accelerates photo-oxidative degradation at 60 °C.

Representative stress–strain curves for UV-aged and HUV-aged films are compared in Figs. 1 and 2. Plots for films with 48 h of UV exposure are shown in Fig. 1 and plots for films with 96 h of UV exposure are shown in Fig. 2. The subplots in Figs. 1 and 2 show results at different strain rates.[2] The stress–strain curves in Figs. 1 and 2 show that the initial linear response between the true stress and strain is brief. Afterwards, the true stress gradually rolls over up to the yield point and then exhibits approximately linear hardening until fracture. For both UV and HUV aging, scatter in strength was low while scatter in strain-to-fracture was high, so representative stress–strain curves are useful for exploring the trends with strength, but not strain-to-fracture. For UV-aged and HUV-aged specimens with the same UV exposure time and tested at the same strain rate, no difference in strength is apparent. In other words, the UV-aged and HUV-aged films follow roughly the same stress–strain path until fracture.

Since the scatter in strain-to-fracture is high, the entire data set must be examined to determine if hygrothermal aging had any influence on ductility. The strain-to-fracture versus UV exposure time for three different strain rates is shown in Fig. 3. As expected, the average strain-to-fracture is lower for films with 96 h of UV exposure time than for films with 48 h of UV exposure time. However, when comparing UV-aged and HUV-aged films with the same UV

[2] The effect of strain rate was not within the scope of this study, but different strain rates were nevertheless used to build a data set suitable for calibrating a viscoplastic model [35].

Fig. 2 Representative stress–strain curves for PA-6 films aged by UV (blue, solid line) or by alternating UV and hygrothermal conditions (HUV, orange, dashed line). Markers indicate the strain-to-fracture. All specimens were UV-aged for 96 h. Each plot shows results from tests using the same nominal strain rate. The hygrothermal exposure had no apparent effect on the strength of the films

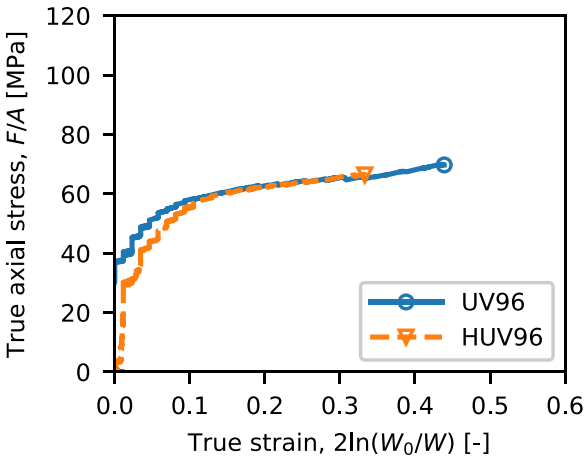

(a) $\dot{\delta}/L_0 = 10^{-3}/\mathrm{s}$

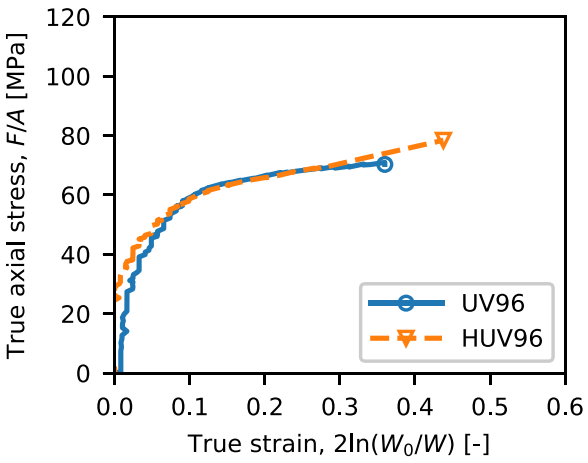

(b) $\dot{\delta}/L_0 = 10^{-2}/\mathrm{s}$

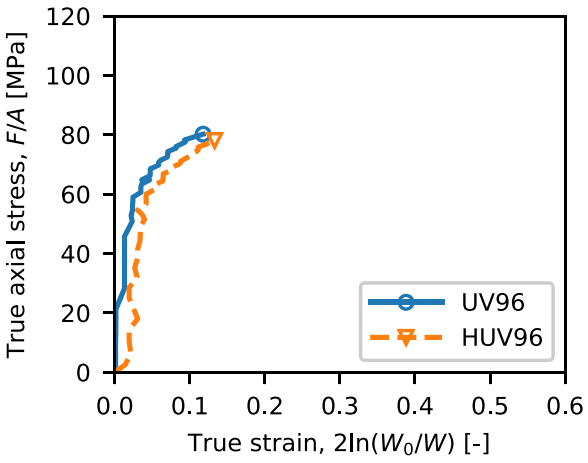

(c) $\dot{\delta}/L_0 = 10^{-1}/\mathrm{s}$

exposure time and strain rate, no clear trends emerge. Given that much of the data is spread out over several strain rates, it is useful to account for the effect of strain rate on ductility and then re-evaluate the effect of hygrothermal aging on the ductility using a larger sample size of film specimens. The effect of strain rate on the ductility of the film specimens is shown in Fig. 4. For both the UV48-aged and HUV48-aged films in Fig. 4a and the UV96-aged and HUV96-aged films in Fig. 4b, the strain-to-fracture is apparently insensitive to the strain rate. Linear regressions for both UV and HUV films are fit to the data using the log of the strain rate as the independent variable. The slopes of these regressions are nearly flat for all four aging conditions (UV48, HUV48, UV96, HUV96). Nevertheless, to account for any effects of strain rate on the strain-to-fracture, the linear regressions were used to shift all the strain-to-fracture measurements to a strain rate of 10^{-3}/s. In Fig. 5, the shifted strain-to-fracture measurements are plotted for UV and HUV aging as functions of the UV exposure time, allowing for a more statistically meaningful sample size. The larger markers in Fig. 5 represent the average strain-to-fracture for an aging condition, error bars represent the standard deviation, and small markers show individual measurements. Figure 5 clearly shows that the strain-to-fracture decreases with UV exposure time, but no effect of hygrothermal aging is apparent, indicating that the loss of ductility is dominated by UV aging.

Bulk specimens

Next, consider the mechanical behavior of UV-aged and HUV-aged cylindrical (bulk) specimens. The cylindrical specimens have a radius of 2.38 mm, but the depth of oxidative damage is likely on the order of 100 μm [10, 19, 46] due to diffusion-limited oxidation. On the other hand, PA-6 is hygroscopic, so moisture will more readily diffuse through the volume [47]. In a study on diffusion-limited hydrolysis (DLH), Linde et al. [44] estimated that the critical thickness for DLH in PA-6 at 60 °C is 2 cm, well above even the thickness of the present bulk specimens.

A previous study [20] explored the effect of photo-oxidation on the mechanical behavior of PA-6 using the same bulk material and aging procedures as the present study. That study found that, because of the limited thickness of oxidation due to DLO, the average strength was unaffected, so the aged and unaged specimens followed essentially the

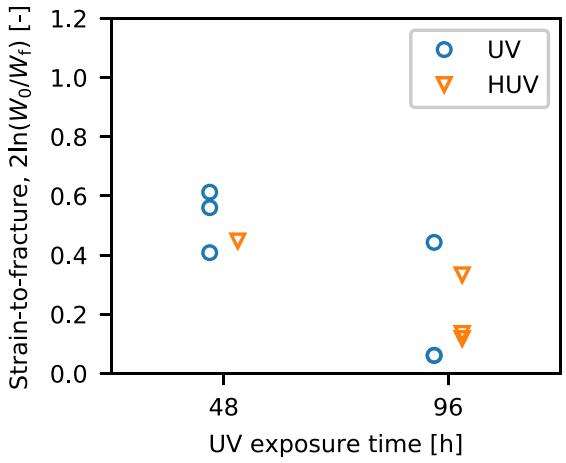

(a) $\dot{\delta}/L_0 = 10^{-3}/\mathrm{s}$

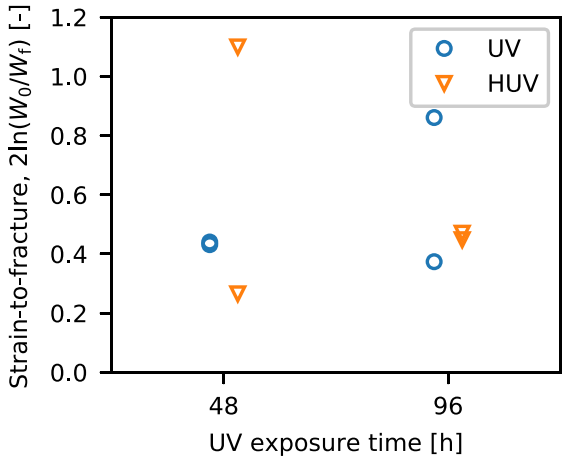

(b) $\dot{\delta}/L_0 = 10^{-2}/\mathrm{s}$

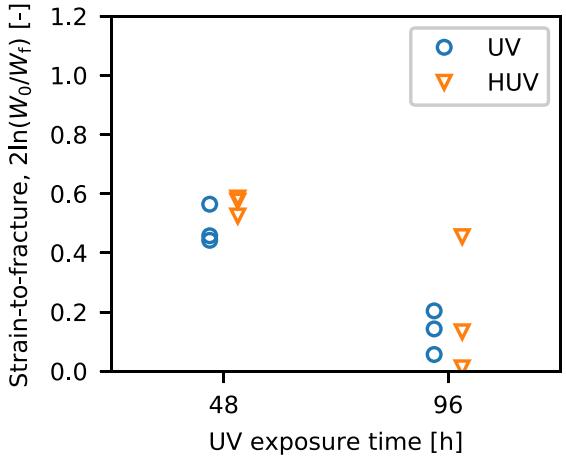

(c) $\dot{\delta}/L_0 = 10^{-1}/\mathrm{s}$

Fig. 3 Strain-to-fracture versus UV exposure time for PA-6 films aged by UV (blue circles) or by alternating UV and hygrothermal conditions (HUV, orange triangles). Each plot shows results from tests using the same nominal strain rate. Small horizontal offsets are applied to markers for clarity

same stress–strain curve up to the initiation of fracture. In the unaged specimens, fracture occurred only after extensive necking and cold drawing. In the aged specimens, fracture occurred at much lower strains and was mediated by the formation of a macro-crack in the oxidized surface that propagated through the thickness as the specimen was drawn.

Representative stress–strain curves comparing the mechanical behavior of the UV-aged and HUV-aged bulk specimens are plotted in Fig. 6. The yield point, defined here as the limit of proportionality, is much clearer in the bulk specimens than in the film specimens. Beyond yield, the material exhibits a slight double-yield behavior [48, 49] and monotonically hardens up to fracture initiation. Figure 6a shows stress–strain curves for UV-aged and HUV-aged bulk specimens exposed to UV for 48 h. Here, the mechanical behavior is essentially the same for the specimens aged under the UV48 and HUV48 conditions. Figure 6b shows that the HUV96 specimen is slightly softer than the UV96 specimen. The difference in strength is even greater for the UV192 and HUV192 specimens (see Fig. 6c). The HUV48, HUV96, and HUV192 specimens were hygrothermally aged for 24 h, 48 h, and 96 h, respectively (see Table 1), so increasing the hygrothermal aging time decreases the strength of PA-6. The effect of UV and hygrothermal aging on the strength is further explored by plotting the yield stress in Fig. 7a. Figure 7a shows that the yield stress was constant with aging time when the bars were only aged by UV. This is expected in bulk specimens, since the limited depth of photo-oxidation does not affect the average strength, at least until cracks eventually initiate from the oxidized surface and propagate through the thickness [20, 37]. On the other hand, the yield stress of the HUV-aged specimens (dried for 72 h) decreases with increasing aging time. However, since the mechanical behavior of the PA-6 films was unaffected by hygrothermal aging, it seems unlikely that the decrease in strength is related to chemical changes from hydrolysis or some coupling between oxidation and moisture. Instead, the decreasing yield stress in the bulk specimens is caused by increased moisture uptake during hygrothermal aging, since absorbed moisture is known to reduce the strength of PA-6 [43]. Decreasing strength due to moisture uptake did not manifest in the films because they were thin enough that 72 h in a vacuum oven dried them completely. For the bulk specimens not exposed to hygrothermal aging, 72 h was also sufficient for drying (see the Appendix). However, for the increased moisture content in the HUV-aged specimens, 72 h was not

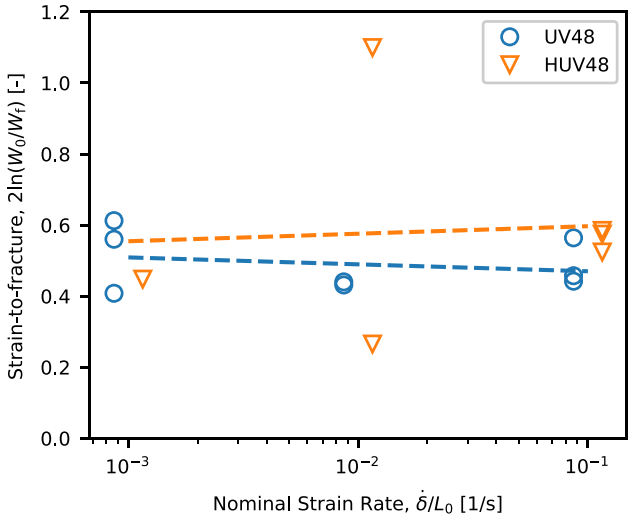

(a) UV48 and HUV48

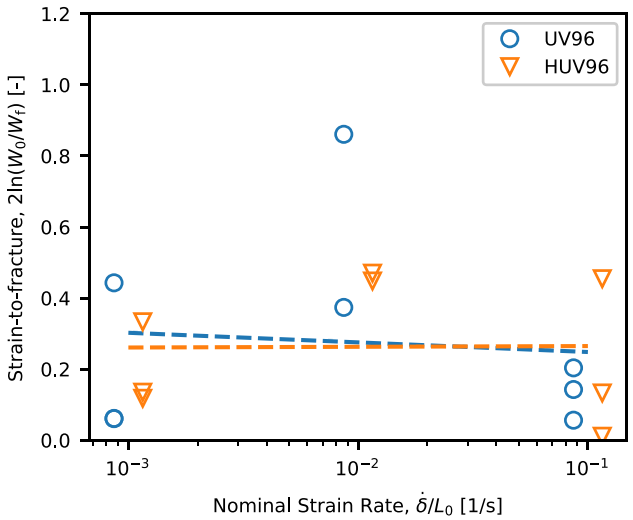

(b) UV96 and HUV96

Fig. 4 Effect of the nominal strain rate on the strain-to-fracture of PA-6 films aged by either UV or HUV. Experimental measurements (markers) and linear regressions (dashed lines) are included. The strain-to-fracture is relatively insensitive to the nominal strain rate

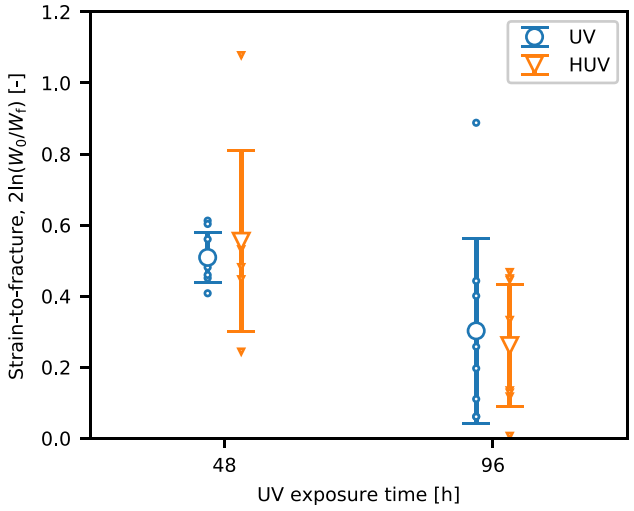

Fig. 5 Strain-to-fracture for all film specimens after accounting for the effect of the strain rate using linear regressions. Individual experimental measurements (small markers) are plotted alongside the average values (large markers). Error bars represent one standard deviation from the average. The hygrothermal exposure had no apparent effect of the strain-to-fracture of the films

sufficient to dry the specimen, so the strength decreased with increasing hygrothermal exposure.

To confirm that the reduced strength in the HUV-aged specimens was related to moisture uptake rather than hydrolysis, HUV-aged specimens were dried for twice as long (144 h) and then mechanically tested. Stress–strain curves for the HUV-aged specimens dried for 144 h are plotted alongside results for UV-aged and HUV-aged specimens dried for 72 h in Fig. 6, where it is seen that HUV-aged specimens dried for 144 h exhibit essentially the same mechanical behavior as the specimens aged by UV only. Figure 7a corroborates this, as it shows that hygrothermal aging has no effect on the yield stress when the drying time is increased from 72 to 144 h.

The strain-to-fracture versus UV exposure time is plotted in Fig. 7b. As with the film specimens, there is high scatter for the strain-to-fracture of the bulk specimens. When a thick specimen is aged by UV radiation, the limited diffusion of oxygen confines the oxidation reactions to a relatively thin surface of the specimen. When a load is applied, cracks initiate in the aged surface and then propagate into the unaged core [20]. In this way, photo-oxidation reduces the ductility of a thick bar, even though a high fraction of the volume is essentially unaged. Therefore, it is not surprising that Fig. 7b shows that strain-to-fracture decreases with increasing UV exposure. All aging conditions (UV only, HUV with 72 h drying, and HUV with 144 h drying) show essentially the same strain-to-fracture for a given UV exposure time. Although Fig. 7b does not show any significant difference between the ductility of UV-aged and HUV-aged bulk specimens, there were admittedly a small number of bulk specimens tested. However, because this conclusion is also supported by the larger sample size of films shown in Fig. 5, it seems unlikely that the lack of an effect exhibited by the bulk specimens is just a statistical quirk arising from a small sample size. Therefore, it seems likely that, with regard to ductility, the effect of hygrothermal aging on bulk PA-6 was insignificant compared to photo-oxidation.

As further confirmation that HUV aging only changes the mechanical behavior of the cylindrical bars through increased moisture uptake, an unaged cylindrical bar and an HUV192-aged bar were dried in the vacuum oven and

Fig. 6 Representative stress–strain curves for PA-6 cylindrical bars aged by UV (blue, solid line), by alternating UV and hygrothermal conditions (HUV dried 72 h, orange, dashed line), or by alternating UV and hygrothermal conditions with an extended drying time (HUV dried 144 h black, dotted line). Markers indicate the strain-to-fracture. All specimens were loaded at a nominal strain rate of $\dot{\delta}/L_0 = 10^{-3}/\text{s}$. Each plot shows results for specimens aged with the same UV exposure time

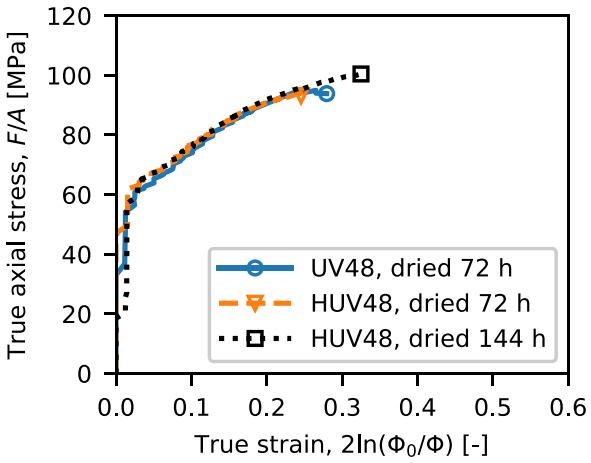

(a) 48 h of UV

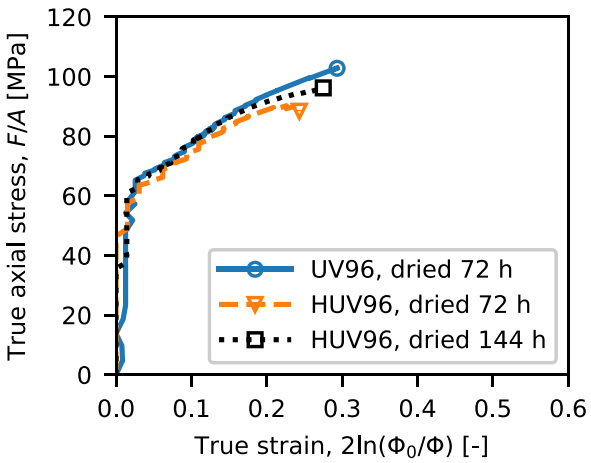

(b) 96 h of UV

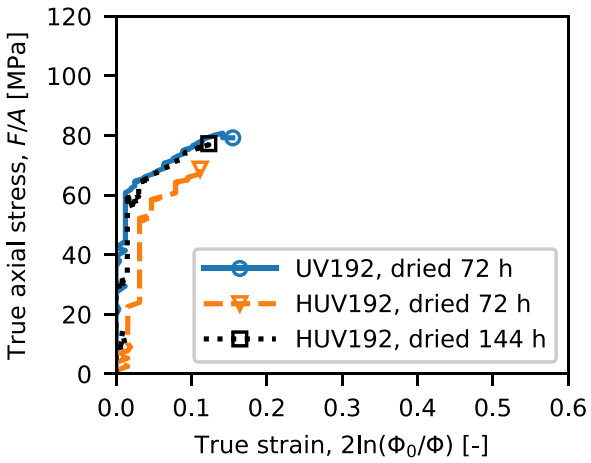

(c) 192 h of UV

Discussion

After accounting for plasticization by absorbed water, the strength and strain-to-fracture of PA-6 changed only from UV exposure. The additional hygrothermal aging had no effect. This result is somewhat surprising in the context of the limited number of studies on coupling between oxidation and moisture. Thermo-oxidation and photo-oxidation follow similar reaction schemes [10, 11, 28, 31], and several studies in the literature show that moisture accelerates chemical degradation of polyamides [23–25, 30, 31]. However, of these studies, two focus on PA-6 with additives [23, 30], and thus, the primary aging mechanism in those studies is hydrolysis, rather than oxidation (as in the present study). The other three studies examine coupling between oxidation and moisture using only chemical measurements [24, 25, 31]. Only one of these references studies coupling between photo-oxidation and moisture [24]. Thus, to the author's knowledge, this paper is the first study on the effects of combined hygrothermal and photo-oxidative aging on the mechanical properties of additive-free PA-6.

It remains to be explained how the present results can be reconciled with other findings that thermo-oxidation is accelerated by moisture [25]. By measuring carbonyl absorbance, Gijsman [24] also found that moisture had no effect on the photo-oxidation of PA-6. The aging procedure employed by Gijsman used a Xenon light source emitting UV with an irradiance of (0.35 W/m^2·nm) at the peak wavelength of 340 nm under a temperature of 64 °C, following the protocol of ASTM G155-00 [50]. Gijsman used continuous illumination with a dry/wet cycle of 102 min dry and 18 min of front water spray. For comparison, the aging procedure for the present study used fluorescent UV lamps with an irradiance

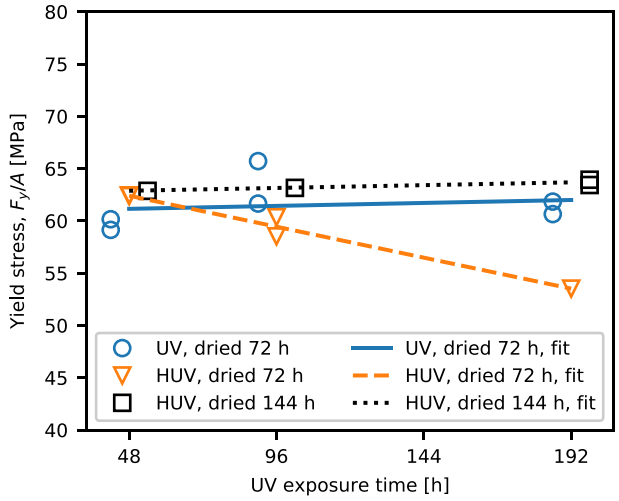

(a) Yield stress

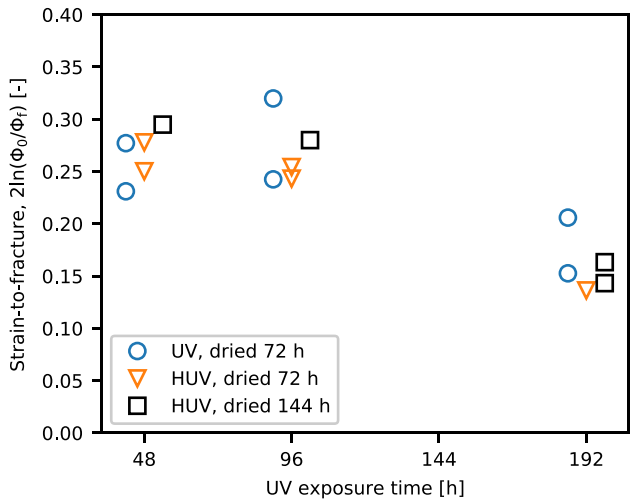

(b) Strain-to-fracture

Fig. 7 **a** Yield stress and **b** strain-to-fracture versus UV exposure time for PA-6 cylindrical bar specimens. Data includes specimens aged by UV (blue circles), by alternating UV and hygrothermal conditions (HUV dried 72 h, orange triangles), or by alternating UV and hygrothermal conditions with an extended drying time (HUV dried 144 h, black squares). Small horizontal offsets are applied to markers for clarity. In **a**, linear fits to the data are included to guide the eye. Hygrothermal aging had no effect on the strain-to-fracture, but decreased the yield stress. However, the effects of hygrothermal aging on the mechanical behavior were reversible when the length of the vacuum drying procedure was doubled

of (1.55W/m^2·nm) at the peak wavelength of 340nm under a temperature of 60 °C, following a protocol based on ASTM-G154-12a [36]. In the present study, the UV lamps were on for 24 h under dry conditions followed by 4 h with the lamps off at 100 °C RH. Both the present study and Gijsman [24]

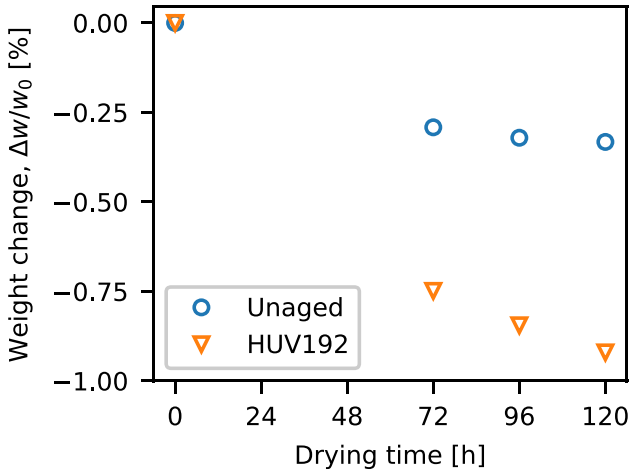

Fig. 8 Change in weight during the vacuum drying procedure for an unaged (blue circles) and an HUV192-aged (orange triangles) PA-6 cylindrical bar. It is assumed that the main mechanism for weight loss is the removal of moisture from the specimen. The HUV-aged specimen continues to lose significant weight beyond 72 h, indicating that the original drying procedure was not sufficient to dry the HUV-aged specimens

use nearly the same aging temperatures, UV wavelengths, and ratios of dry to wet time (approximately 6 min of dry time per 1 min of wet time). However, Gijsman [24] uses a lower UV irradiance and continuous illumination, while the present study alternated between UV radiation with ambient humidity and no UV radiation with 100% RH. The similarities between this study and [24] demonstrate that the finding that moisture has no effect on the photo-oxidation of PA-6 is repeatable for the aging conditions chosen based on ASTM-G154-12a [36] and ASTM G155-00 [50]. However, this study complements Gijsman [24] by quantifying degradation using mechanical properties, while Gijsman [24] arrives at the same conclusion using evidence of chemical reactions (carbonyl absorbance).

In the present study, hygrothermal aging at 100% RH was interspersed between periods of UV exposure at ambient humidity, so the PA-6 specimens were never simultaneously exposed to both UV radiation and 100% RH. However, alternating between the two aging conditions is unlikely to eliminate the possibility for coupled degradation pathways. Deshoulles et al. [25] showed nonlinear coupling between oxidation and hydrolysis of PA-6 for both simultaneous exposure to water and air as well as a staggered procedure where PA-6 was oxidized in air without water followed by hydrolysis in water without air. Specifically, pre-oxidized PA-6 held in water without air showed a higher chain scission concentration from hydrolysis compared to PA-6 held in water without air and no pre-oxidation treatment. In [25], the authors

hypothesized that the pre-oxidation left behind imides that created additional reactive sites for hydrolysis. Their experiment demonstrates that oxidation followed by moisture still allows for the possibility of coupled degradation in PA-6. Gonçalves et al. [31] proposed that oxidation is accelerated by moisture because moisture is absorbed into the PA-6 and increases the chain mobility. In the present study, the hygrothermally aged specimens showed decreased strength that was reversed by increasing drying time before mechanical loading (see Fig. 7a). This is evidence that the hygrothermally aged specimens absorbed and retained more water than the specimens aged by UV-only (see Fig. 8). Therefore, elevated moisture content is expected after each hygrothermal cycle, so coupling between photo-oxidation and moisture is possible even when the hygrothermal aging proceeds with the UV exposure. Also, the previously mentioned presentation by Gijsman [24] did subject PA-6 to simultaneous UV and moisture and still found no effect of moisture on photo-oxidation. Altogether, it seems unlikely that the lack of coupling between photo-oxidation and moisture in PA-6 is due to staggering the UV and moisture exposure.

However, this study used an aging temperature of 60 °C, which is relatively low compared to other studies on coupled moisture and thermo-oxidation. Bernstein and Gillen [23] inferred that moisture would not influence the degradation of PA-6,6 in air at temperatures below 50 °C. However, their studies used PA-6,6 fibers with antioxidants, so degradation in their experiments was due to hydrolysis rather than oxidation. Nevertheless, there is also likely a temperature at which oxidation is not accelerated by moisture, and 60 °C may be near or below that temperature. The lowest temperatures used for combined oxidative and hygrothermal aging in [25] was 80 °C and the lowest combined aging temperature in [31] was 70 °C. Perhaps moisture would also accelerate photo-oxidation at these higher temperatures. However, given that 60 °C is a conservative upper limit for natural air temperatures on Earth, the results from this study and from [24] indicate that the effect of moisture on the degradation of PA-6 is negligible compared to the effect of UV radiation. Of course, for polymers like polyamides that are hygroscopic and plasticized by water, only the chemical effects of moisture can be neglected.

Conclusion

Coupling between hygrothermal aging and UV-induced photo-oxidative aging was investigated via the mechanical behavior of bulk and film specimens of additive-free PA-6. This is the first study that reports the mechanical behavior of PA-6 aged after combined hygrothermal and photo-oxidative aging.

For the film specimens, the strength and ductility were only dependent on the UV exposure times; the hygrothermal aging had no effect on photo-oxidative degradation. For bulk specimens, the ductility was also insensitive to hygrothermal aging, but the strength decreased with hygrothermal aging. However, the loss of strength was reversible by extending the pre-loading vacuum drying time, demonstrating that the loss of strength was related to the plasticization of PA-6 by absorbed water rather than from chemical aging related to coupling between water and photo-oxidation.

Because the additional hygrothermal aging had no irreversible effects on the mechanical behavior of either film or bulk specimens, it can be concluded that (1) chemical degradation from hygrothermal aging at 60 °C was negligible compared to that from photo-oxidation and (2) that chemical coupling between these two environmental factors is unimportant at 60 °C. These findings are inconsistent with other studies, where strong coupling was found between moisture and thermo-oxidation of additive-free PA-6. However, studies showing coupling were conducted at higher temperatures. Therefore, it seems likely that mechanisms for coupling between moisture and oxidation in PA-6 accelerate at some temperature above 60 °C. Future investigations should explore the temperature where coupling between hygrothermal and photo-oxidation becomes relevant for PA-6.

Appendix: Hygroscopic aging of PA-6

PA-6 is hygroscopic, meaning it readily absorbs moisture [41, 42]. The absorbed moisture acts as a plasticizer that reduces the glass transition temperature and strength while increasing the ductility [41]. For this reason, the experimental protocol included a vacuum drying procedure as described in Section 2.3. The vacuum drying procedure was chosen based on preliminary studies on round notched bars loaded to failure after various storage times in a desiccant, but without any pre-test vacuum drying. The round notched bars had a notch root diameter and notch radius of 3.90 mm, a notch shoulder diameter of 7.00 mm, a gauge length of 6.22 mm, and a total length of 57.50 mm. The notched bar geometry was chosen to study triaxiality effects in photo-oxidized PA-6 for a publication in preparation and can be designated as RN10 specimens following the nomenclature for round notched bars used in [51, 52]. These specimens were stored in a cabinet with a tray of calcium sulfate ($CaSO_4$) desiccant after being machined from a cast plate of PA-6. When the desiccant was saturated, indicated by a change in color from light blue to purple, it was changed. The ambient humidity in the laboratory where the cabinet was located was typically $60 \pm 5\%$, although measurements as low as $50 \pm 5\%$ and as high as $70 \pm 5\%$ were recorded. These specimens were not aged by either UV or

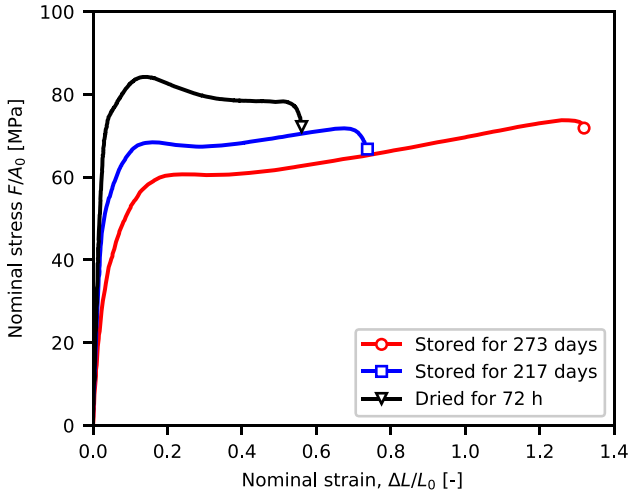

Fig. 9 Nominal stress–strain curves for PA-6 RN10 bars that were loaded after being stored in a chamber with a desiccant ($CaSO_4$) or were loaded immediately after drying in a vacuum oven. Markers represent the strain-to-fracture. Moisture absorbed during storage increased the ductility and decreased the strength

hygrothermal aging, so any changes in their mechanical properties with time are an effect of hygroscopic aging, i.e., changes caused by the absorption of moisture under ambient conditions. The specimens were loaded in displacement control mode on an MTS Insight Electromechanical Testing System. The test frame was instrumented with a 30-kN load cell and a laser extensometer. The nominal axial stress was calculated as $\sigma = F/A_0$, where F is the force measured by the load cell and A_0 is the initial cross-sectional area at the notch root (narrowest point in the notch). The nominal strain was calculated as $\Delta L/L_0$, where ΔL is the displacement measured by the laser extensometer and L_0 is the initial gauge length, defined as the axial length of the notch from shoulder to shoulder.

Figure 9 shows nominal stress–strain curves up to the strain-to-fracture for RN10 bars that were loaded without being dried. A single realization of a bar that was dried prior to loading is also shown for reference. The storage time in the legend is measured from the receipt of the raw material. For increasing storage times, specimens show increasing ductility and decreasing strength, which are the anticipated signatures for moisture absorption [43]. It is notable that the ambient temperature and humidity were able to effect significant changes in the mechanical behavior of PA-6 over a time period of only 60 days. When the specimens were dried prior to loading, the reverse trends were observed (ductility decreased, strength increased), indicating that moisture was removed. The stress–strain curve of the material dried for 72 h was repeatable regardless of the storage time, so that drying time was adopted in the experimental procedure.

Fig. 10 An undeformed PA-6 RN10 bar (left). A PA-6 RN10 bar loaded past the peak nominal stress after storage for 217 days with a desiccant ($CaSO_4$) (center). A PA-6 RN10 bar loaded to fracture after storage for 217 days with a desiccant (right). After absorbing ambient moisture during storage, the material was ductile enough that the notches in the specimen became locally cylindrical during loading

Figure 10 shows images of RN10 bars that were loaded after storage for 217 days. An undeformed RN10 bar is also shown for reference. These images show that the increased ductility allowed the undried notched bars to deform until the notch became smooth, i.e., locally cylindrical. The transition from a shallow notch to a smooth notch represents a significant change in triaxiality: from 0.56 to 1/3. In this case, round notched bars are clearly not suitable as constant triaxiality specimens, complicating their use with ductile polymers to explore the effects of the stress state on the mechanical behavior and damage.

Rozanski and Galeski [43] reported that moisture and other low molecular weight penetrants could suppress cavitation in PA-6. This must be at least partially responsible for the increased ductility in the undried specimens. However, since the necked regions of the specimens in Fig. 10 exhibit stress-whitening, cavitation must have still occurred [53, 54].

Therefore, constitutive models seeking to predict fracture in PA-6 will need to include mechanisms for how moisture affects both the mechanical behavior and damage evolution.

Acknowledgements This work is based on research from KNC's Ph.D. dissertation [51]. KNC is presently affiliated with Sandia National Laboratories. Sandia National Laboratories is a multi-mission laboratory managed and operated by National Technology & Engineering Solutions of Sandia, L.L.C. (NTESS), a wholly owned subsidiary of Honeywell International, Inc., for the U.S. Department of Energy's National Nuclear Safety Administration (DOE/NNSA) under contract DE-NA0003525. This written work is authored by an employee of NTESS. The employee, not NTESS, owns the right, title, and interest in and to the written work and is responsible for its contents. Any subjective views or opinions that might be expressed in the written work do not necessarily represent the views of the US government. The publisher acknowledges that the US government retains a non-exclusive, paid-up, irrevocable, worldwide license to publish or reproduce the published form of this written work or allow others to do so, for the US government purposes. The DOE will provide public access to results of federally funded sponsored research in accordance with the DOE Public Access Plan.

Author contribution AAB designed the research; KNC and AKR carried out the experiments; KNC prepared all figures and prepared the initial draft of the manuscript; and KNC, AKR, and AAB contributed to the analysis of the results, reviewing the manuscript, and revising the manuscript.

Funding This research was supported by the Qatar National Research Fund (NPRP grant no. 7-1562-2-571).

Availability of data and materials The data presented in this article will be made available upon reasonable request to the corresponding author.

Declarations

Ethical approval Not applicable. The results published in this article did not involve the study of humans or animals.

Competing interests The authors declare no competing interests.

References

1. Cummings CS, Lucas EM, Marro JA, Kieu TM, DesJardins JD (2011) The effects of proton radiation on UHMWPE material properties for space flight and medical applications. Adv Space Res 48:1572–1577
2. Lytle CD, Sagripanti J-L (2005) Predicted inactivation of viruses of relevance to biodefense by solar radiation. J Virol 79:14244–14252
3. Laügt C, Bouvard J-L, Robert G, Billon N (2022) Thermo-hydro-glycol ageing of polyamide 6,6: microstructure-properties relationships. Polymers 14:4097
4. George GA (1995) Weathering of polymers. Mater Forum 19:145–161
5. Feldman D (2002) Polymer weathering: photo-oxidation. J Polym Environ 10:163–173
6. Qayyum MM, White JR (1986) The effect of weathering on residual stresses and mechanical properties in injection-moulded semi-crystalline polymers. J Mater Sci 21:2391–2402
7. Qayyum M, White J (1987) Plastic fracture in weathered polymers. Polymer 28:469–476
8. Arrieta C, Dong Y, Lan A, Vu-Khanh T (2013) Outdoor weathering of polyamide and polyester ropes used in fall arrest equipment. J Appl Polym Sci 130:3058–3065
9. Liu Z et al (2022) Quantifying the dynamics of polystyrene microplastics UV-aging process. Environ Sci Technol Lett 9:50–56
10. Rabek JF (1996) Photodegradation of polymers. Springer, Berlin Heidelberg, Berlin, Heidelberg
11. Grigg MN (2006) Thermo-oxidative degradation of polyamide 6. Ph.D. thesis, Queensland University of Technology, Brisbane, Australia
12. El-Mazry C, BenHassine M, Correc O, Colin X (2013) Thermal oxidation kinetics of additive free polyamide 6-6. Polym Degrad Stab 98:22–36
13. El-Mazry C, Correc O, Colin X (2012) A new kinetic model for predicting polyamide 6–6 hydrolysis and its mechanical embrittlement. Polym Degrad Stab 97:1049–1059
14. Celina M, George G (1995) Heterogeneous and homogeneous kinetic analyses of the thermal oxidation of polypropylene. Polym Degrad Stab 50:89–99
15. Fayolle B, Audouin L, Verdu J (2000) Oxidation induced embrittlement in polypropylene — a tensile testing study. Polym Degrad Stab 70:333–340
16. Fayolle B, Colin X, Audouin L, Verdu J (2007) Mechanism of degradation induced embrittlement in polyethylene. Polym Degrad Stab 92:231–238
17. Fayolle B, Richaud E, Colin X, Verdu J (2008) Review: Degradation-induced embrittlement in semi-crystalline polymers having their amorphous phase in rubbery state. J Mater Sci 43:6999–7012
18. Celina MC (2013) Review of polymer oxidation and its relationship with materials performance and lifetime prediction. Polym Degrad Stab 98:2419–2429
19. Gijsman P, Dong W, Quintana A, Celina M (2016) Influence of temperature and stabilization on oxygen diffusion limited oxidation profiles of polyamide 6. Polym Degrad Stab 130:83–96
20. Cundiff KN, Madi Y, Benzerga AA (2020) Photo-oxidation of semicrystalline polymers: damage nucleation versus growth. Polymer 188:122090
21. Rodriguez AK, Mansoor B, Ayoub G, Colin X, Benzerga AA (2020) Effect of UV-aging on the mechanical and fracture behavior of low density polyethylene. Polym Degrad Stab 180:109185
22. Deshoulles Q et al (2021) Origin of embrittlement in Polyamide 6 induced by chemical degradations: mechanisms and governing factors. Polym Degrad Stab 191:109657
23. Bernstein R, Gillen KT (2010) Nylon 6.6 accelerating aging studies: II. Long-term thermal-oxidative and hydrolysis results. Polym Degrad Stab 95:1471–1479
24. Gijsman P (2014) The unexpected importance of humidity on the thermo-oxidative and photo-oxidative degradation of polyamides, in: Proceedings of the 8th International Conference on Modification, Degradation and Stabilization of Polymers. Portoroz, Slovenia
25. Deshoulles Q et al (2022) Chemical coupling between oxidation and hydrolysis in polyamide 6 - a key aspect in the understanding of microplastic formation. Polym Degrad Stab 197:109851
26. Satoto R et al (1997) Weathering of high-density polyethylene in different latitudes. Polym Degrad Stab 56:275–279
27. Xiong J et al (2017) Natural weathering mechanism of isotatic polypropylene under different outdoor climates in China. Polym Degrad Stab 146:212–222
28. Lemaire J, Arnaud R, Gardette J-L (1991) Low temperature thermo-oxidation of thermoplastics in the solid state. Polym Degrad Stab 33:277–294
29. Roger A, Sallet D, Lemaire J (1986) Photochemistry of aliphatic polyamides. 4. Mechanisms of photooxidation of polyamides 6, 11, and 12 at long wavelengths. Macromolecules 19:579–584
30. Bernstein R, Derzon DK, Gillen KT (2005) Nylon 6.6 accelerated aging studies: thermal–oxidative degradation and its interaction with hydrolysis. Polym Degrad Stab 88:480–488

31. Gonçalves ES, Poulsen L, Ogilby PR (2007) Mechanism of the temperature-dependent degradation of polyamide 66 films exposed to water. Polym Degrad Stab 92:1977–1985
32. Arash B, Thijsse B, Pecenko A, Simone A (2017) Effect of water content on the thermal degradation of amorphous polyamide 6,6: a collective variable-driven hyperdynamics study. Polym Degrad Stab 146:260–266
33. Bahrololoumi A, Morovati V, Shaafaey M, Dargazany R (2021) A multi-physics approach on modeling of hygrothermal aging and its effects on constitutive behavior of cross-linked polymers. J Mech Phys Solids 156:104614
34. Ishida T, Kitagaki R, Hagihara H, Elakneswaran Y (2021) Role of moisture in photo-ageing -macromolecular architecture evolution of acrylic-urethane network. Polym Test 96:107123
35. Cundiff KN, Ayoub G, Benzerga AA (2022) Modeling the viscoplastic behavior of a semicrystalline polymer. Int J Solids Struct 254–255:111920
36. Subcommittee G03.03 (2012) Practice for operating fluorescent ultraviolet (UV) lamp apparatus for exposure of nonmetallic materials. Standard ASTM G154-12a, ASTM International, West Conshohocken, PA
37. Wei X-F et al (2018) Diffusion-limited oxidation of polyamide: three stages of fracture behavior. Polym Degrad Stab 154:73–83
38. Gillen KT, Clough RL (1992) Rigorous experimental confirmation of a theoretical model for diffusion-limited oxidation. Polymer 33:4358–4365
39. Rodriguez AK (2020) Characterization and mechanical modeling of UV-aged semicrystalline polymers. Ph.D. thesis, Texas A &M University, College Station, TX
40. El Chaar L, Lamont LA (2010) Global solar radiation: multiple on-site assessments in Abu Dhabi, UAE. Renew Energy 35:1596–1601
41. Kohan MI (1973) Nylon plastics SPE monographs. Wiley, New York
42. Biron M (2007) Thermoplastics and thermoplastic composites: technical information for plastics users. Elsevier, Amsterdam Heidelberg
43. Rozanski A, Galeski A (2013) Plastic yielding of semicrystalline polymers affected by amorphous phase. Int J Plast 41:14–29
44. Linde E, Giron NH, Celina MC (2022) Diffusion-limited hydrolysis in polymeric materials. Polym Degrad Stab 204:110095
45. Cunliffe A, Davis A (1982) Photo-oxidation of thick polymer samples—Part II: The influence of oxygen diffusion on the natural and artificial weathering of polyolefins. Polym Degrad Stab 4:17–37
46. Rodriguez AK, Mansoor B, Benzerga AA (2023) Oxidation-induced stiffening versus weakening in semicrystalline polymers. J Mater Sci
47. Jia N, Fraenkel HA, Kagan VA (2004) Effects of moisture conditioning methods on mechanical properties of injection molded nylon 6. J Reinf Plast Compos 23:729–737
48. Razavi M, Wang S-Q (2020) Double yielding in deformation of semicrystalline polymers. Macromol Chem Phys 221:2000151
49. Shan G-F et al (2007) Effect of temperature and strain rate on the tensile deformation of polyamide 6. Polymer 48:2958–2968
50. Subcommittee G03.03 (2000) Standard practice for operating xenon arc light apparatus for exposure of non-metallic materials. Standard ASTM G155-00, ASTM International, West Conshohocken, PA
51. Cundiff KN (2020) Experimental characterization and modeling of aging-induced damage in semicrystalline thermoplastics. Ph.D. thesis, Texas A &M University, College Station, TX
52. Kondori B, Benzerga AA (2014) Effect of stress triaxiality on the flow and fracture of Mg alloy AZ31. Metall and Mater Trans A 45:3292–3307
53. Pae KD, Chu H-C, Lee JK, Kim J-H (2000) Healing of stress-whitening in polyethylene and polypropylene at or below room temperature. Polym Eng Sci 40:1783–1795
54. Lee JK, Kim JH, Chu H-C, Pae KD (2002) Macroscopic observation of healing process in stress-whitened polypropylene under hydrostatic pressure. Polym Eng Sci 42:2351–2360